Stochastic predictive control of autonomous vehicles in uncertain environments

Conference Paper · September 2014

CITATIONS
36

READS
1,991

4 authors, including:

Ashwin Carvalho
University of California, Berkeley
24 PUBLICATIONS **408** CITATIONS
SEE PROFILE

Yiqi Gao
University of California, Berkeley
16 PUBLICATIONS **635** CITATIONS
SEE PROFILE

Stephanie Lefevre
Mercedes Benz Research and Development North America
32 PUBLICATIONS **820** CITATIONS
SEE PROFILE

Stochastic Predictive Control of Autonomous Vehicles in Uncertain Environments

Ashwin Carvalho[a], Yiqi Gao[a], Stéphanie Lefèvre[a], Francesco Borrelli[a]

[a] **University of California at Berkeley, USA**

Berkeley, CA 94720, USA
Phone: +1-510-643-2044
E-mail: ashwinc@berkeley.edu

Autonomous vehicles operating in dynamic urban environments must account for the uncertainty arising from the behavior of other objects in the environment. For this purpose, we develop an integrated environment modeling and stochastic Model Predictive Control (MPC) framework. The trade–off between risk and conservativeness is managed by a risk factor which is a parameter in the control design process. The environment model consists of an Interacting Multiple Model Kalman Filter to estimate and predict the positions of target vehicles. The uncertain predictions are used to formulate a chance–constrained MPC problem. The overall goal is to develop a framework for safe autonomous navigation in the presence of uncertainty and study the effect of the risk parameter on controller performance. Simulations of an autonomous vehicle driving in the presence of moving vehicles show the effectiveness of the proposed framework.

Topics / Autonomous driving and collision avoidance, Environment modeling

1. INTRODUCTION

Recent advances in sensing, computing and control technologies make autonomous passenger vehicles a viable solution to minimize the number of road accidents and resulting fatalities. Autonomous vehicles must navigate in dynamic urban environments in the presence of other static or moving objects such as vehicles, bicycles and pedestrians. One of the main challenges is to systematically account for the uncertainties due to other objects in the control design process.

Nominal control approaches that do not account for system uncertainties may result in unsafe performance. On the other hand, robust control approaches that deal with worst–case disturbances may be too conservative and computationally expensive. We propose a stochastic MPC framework for controlling autonomous vehicles where the risk of constraint violations is a tunable design parameter. MPC has been shown to be an effective strategy for the automotive control problem as it can handle system constraints, nonlinearities and uncertainties in an unified manner [1]–[3].

Chance–constrained optimization has been studied in the context of autonomous vehicles. The work in [4] addresses the tactical planning problem for autonomous vehicles in uncertain environments. The relative motion between controlled and uncontrolled vehicles is modeled as a jump Markov linear system. Sampling is used to approximate the multimodal distribution of the future system state, and the collision avoidance chance–constraints are approximated by convex bounding functions.

Stochastic MPC was applied to a driver assistance system in [1] using the approach presented in [5] for linear time–invariant (LTI) systems with stochastic disturbances. The time–invariance allows the uncertainty propagation to be performed offline for disturbances with any known distribution. However, vehicle models are nonlinear in general due to the complex tire–road interaction. Hence, we propose modeling the vehicle dynamics as a linear time–varying (LTV) system where the linearization is performed online. Disturbances in the system are modeled as Gaussian to allow for the easy propagation of uncertainties and handling of probabilistic constraints.

In addition to a vehicle dynamics model, a predictive controller requires a model of the dynamic environment in which the vehicle is operating. This is used to incorporate predictions of the behavior of other objects in the decision making process. Previous work by the authors assumes that the future positions of all objects in the environment are known over the prediction horizon [1]–[3]. We aim to relax that assumption by developing an environment modeling framework to forecast the positions of nearby objects. In this paper, we focus on the problem of predicting the positions of surrounding vehicles (denoted as *target vehicles*).

The work in [6] classifies traffic motion prediction approaches into three categories, (1) physics–based, (2) maneuver–based, and (3) interaction–aware. Maneuver–based and interaction–aware models generally involve a higher degree of abstraction, and are suited for relatively long–term predictions. This is accompanied by higher computational costs. Since MPC applies inputs in a receding horizon manner, we choose the class of physics–based approaches. Specifically, an Interacting Multiple Model Kalman Filter (IMM–KF) is used to estimate and predict the positions of target vehicles. The IMM–KF is a hybrid system state estimator popular in target tracking literature [7]. A multiple model algorithm such as the IMM–KF is a natural choice for our application due to the multimodal behavior of target vehicles.

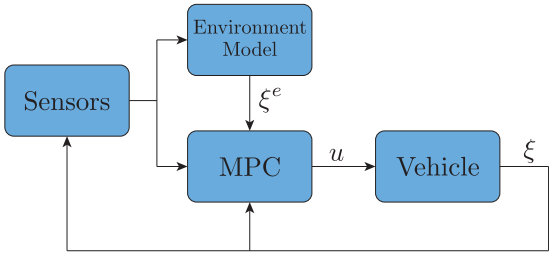

Fig. 1. Block diagram of overall system.

In summary, the overall goals of this work are to (1) develop an integrated environment modeling and probabilistic control framework, and (2) study the trade–off between conservatism and risk for autonomous vehicles through a tunable risk parameter in the chance–constrained MPC. Results from simulations in urban driving scenarios are presented to demonstrate the effectiveness of the proposed framework.

The paper is organized as follows. Section 2 describes the overall architecture of the system. In Section 3, we introduce the environment model to make predictions of target vehicle positions. Section 6 details the formulation of the chance–constrained MPC problem and the stochastic MPC framework. We present simulation results in Section 7 followed by concluding remarks in Section 8.

2. SYSTEM DESCRIPTION

The proposed system architecture is shown in Figure 1. The "Sensors" block is assumed to provide processed information about the vehicle states, road geometry, and relative positions and velocities of target vehicles in real–time. This information is used by the "Environment Model" block to make probabilistic predictions of the positions of target vehicles in the near future. The "MPC" block uses the sensory information along with the forecast evolution of the environment to formulate a chance–constrained receding horizon control problem to optimize the steering and braking inputs to the vehicle. In this work, we focus on developing the "Environment Model" (Section 3) and "MPC" (Section 6) blocks.

3. ENVIRONMENT MODEL

3.1 Target Vehicle Models

The dynamics of the j^{th} target vehicle are described by a Markov jump affine system,

$$\xi^e_{j_{k+1}} = F^{(i)}_k \xi^e_{j_k} + G^{(i)}_k w^{(i)}_k + E^{(i)}_k \tag{1a}$$

$$y^e_{j_k} = H^{(i)}_k \xi^e_{j_k} + v^{(i)}_k, \tag{1b}$$

where $\xi^e_{j_k}$ and $y^e_{j_k}$ denote the target vehicle state and measurement, respectively, at time k. The process noise $w^{(i)}_k$ and measurement noise $v^{(i)}_k$ are assumed to be i.i.d. as $\mathcal{N}(0, Q^{(i)}_k)$ and $\mathcal{N}(0, R^{(i)}_k)$, respectively. The superscript (i) in (1) refers to the model $m^{(i)}$ in the model set $\mathbb{M} = \{m^{(1)}, m^{(2)}, \ldots, m^{(M)}\}$, and transitions between modes have fixed probabilities given by a matrix $\pi \in \mathbb{R}^{M\times M}$, such that

$$\pi_{ij} = P(m_{k+1} = m^{(j)} | m_k = m^{(i)}), \tag{2}$$

where m_k denotes the mode at time k. For the prediction problem, we decouple the longitudinal and lateral motion of the target vehicle. The models used for each are described below. The subscript j and superscript e are dropped for visual clarity.

3.1.1 Longitudinal motion

We choose $\xi = [s, \dot{s}, \ddot{s}]^T$ and $y = [s, \dot{s}]^T$ for the longitudinal state and measurement, respectively. Two modes are used to model the longitudinal motion,

1) Constant velocity:

$$F^{(1)}_k = \begin{bmatrix} 1 & T_s & \frac{T_s^2}{2} \\ 0 & 1 & T_s \\ 0 & 0 & 0 \end{bmatrix} \quad G^{(1)}_k = \begin{bmatrix} \frac{T_s^2}{2} \\ T_s \\ 1 \end{bmatrix}, \tag{3}$$

where T_s is the sampling time.

2) Constant acceleration:

$$F^{(2)}_k = \begin{bmatrix} 1 & T_s & \frac{T_s^2}{2} \\ 0 & 1 & T_s \\ 0 & 0 & 1 \end{bmatrix} \quad G^{(2)}_k = \begin{bmatrix} \frac{T_s^2}{2} \\ T_s \\ 1 \end{bmatrix}. \tag{4}$$

3.1.2 Lateral motion

The target vehicle lateral state and measurement are chosen to be $\xi = [e_y, \dot{e}_y]^T$ and $y = e_y$, respectively. We use state–feedback models to represent the lateral dynamics in typical lane keeping and lane changing maneuvers. The lateral acceleration of the target vehicle with respect to the lane is assumed to evolve as

$$\ddot{e}_{y_k} \approx \frac{\dot{e}_{y_{k+1}} - \dot{e}_{y_k}}{T_s} = -K_2(e_{y_k} - e_{y,ref}) - K_1 \dot{e}_{y_k}. \tag{5}$$

Thus, e_y is assumed to have a second–order response where $[K_1, K_2]$ affect the settling time and overshoot, and $e_y \to e_{y,ref}$. The system matrices are given by

$$F^{(i)}_k = \begin{bmatrix} 1 & T_s \\ -T_s K^{(i)}_2 & 1 - T_s K^{(i)}_1 \end{bmatrix} \tag{6a}$$

$$G^{(i)}_k = \begin{bmatrix} T_s^2/2 \\ T_s \end{bmatrix} \quad E^{(i)}_k = \begin{bmatrix} 0 \\ T_s K^{(i)}_2 e^{(i)}_{y,ref} \end{bmatrix}, \tag{6b}$$

where the superscript (i) denotes the mode. We use a set of nine models (i.e. $M = 9$) corresponding to three different tunings of K_1 and K_2 for each of the lane keeping, lane change left and lane change right maneuvers. Figure 2 shows the trajectories for the 9 modes with initial condition $\xi_0 = [2, 0]^T$, and a lane width of 3 m.

Remark 1: The parameters K_1 and K_2 in (6) are estimated heuristically in this paper. Tools from statistical learning theory may be used to systematically estimate parameters using data.

3.2 IMM–KF Algorithm

At each time step k, we estimate the following quantities based on the current measurement and values at the previous time step:

1) Model probability:

$$\mu^{(i)}_k = P(m_k = i | y_0, \ldots, y_k)$$
$$(i = 1, \ldots, M)$$

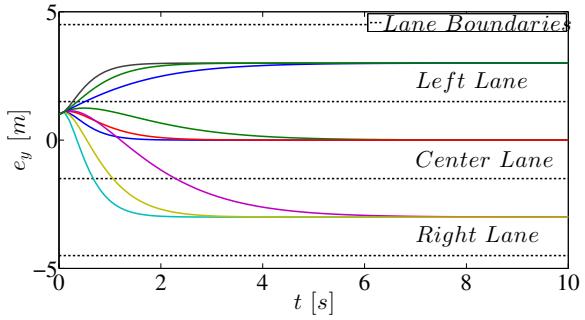

Fig. 2. Predicted trajectories for the target vehicle lateral motion models. The models represent typical maneuvers such as lane keeping, left lane change and right lane change. Variations within a maneuver come from different tunings of the gains K_1 and K_2.

2) Model–conditioned posterior means and covariances (i.e. assuming the mode is time–invariant and equal to i):

$$\hat{\xi}_{k|k}^{(i)} = \mathbb{E}[\xi | y_0, \dots, y_k, m_{k-1} = i, m_k = i]$$
$$\hat{\Sigma}_{k|k}^{(i)} = Cov[\xi | y_0, \dots, y_k, m_{k-1} = i, m_k = i]$$
$$(i = 1, \dots, M)$$

3) Fused posterior mean and covariance:

$$\hat{\xi}_{k|k} = \mathbb{E}[\xi_k | y_0, \dots, y_k]$$
$$\hat{\Sigma}_{k|k} = Cov[\xi_k | y_0, \dots, y_k]$$

The algorithm to compute the above quantities is summarized in [8], and stated below:

Step 1: Evaluate mixing probabilities:

$$\mu_{k-1}^{j|i} = \frac{\pi_{ij}\mu_{k-1}^{(j)}}{\mu_{k|k-1}^{(i)}} \tag{7}$$

$$\text{where } \mu_{k|k-1}^{(i)} = \sum_{j=1}^{M} \pi_{ji}\mu_{k-1}^{(j)}$$

Mixing estimates:

$$\bar{\xi}_{k-1|k-1}^{(i)} = \sum_{j=1}^{M} \hat{\xi}_{k-1|k-1}^{(j)} \mu_{k-1}^{j|i} \tag{8}$$

Mixing covariances:

$$\bar{\Sigma}_{k-1|k-1}^{(i)} = \sum_{j=1}^{M} [\Sigma_{k-1|k-1}^{(j)} + (\bar{\xi}_{k-1|k-1}^{(i)} - \hat{\xi}_{k-1|k-1}^{(i)}) \cdot (\bar{\xi}_{k-1|k-1}^{(i)} - \hat{\xi}_{k-1|k-1}^{(i)})^T] \mu_{k-1}^{j|i} \tag{9}$$

Step 2: For each mode $M^{(i)}$, run Kalman filter with inputs $(\bar{\xi}_{k-1|k-1}^{(i)}, \bar{\Sigma}_{k-1|k-1}^{(i)})$ using Algorithm 1. We obtain the following model–conditioned estimates,

$$(\hat{\xi}_{k|k}^{(i)}, \hat{\Sigma}_{k|k}^{(i)}, \tilde{y}_k^{(i)}, S_k^{(i)})$$

Step 3: Update the probability of each model,

$$\mu_k^{(i)} = \frac{\mu_{k|k-1}^{(i)} \mathcal{N}(\tilde{y}_k^{(i)}; 0, S_k^{(i)})}{\sum_{j=1}^{M} \mu_{k|k-1}^{(j)} \mathcal{N}(\tilde{y}_k^{(j)}; 0, S_k^{(j)})} \tag{10}$$

where $\mathcal{N}(x; \mu, \Sigma)$ is the probability density function of a multivariate normal distribution with mean μ and covariance Σ, evaluated at x.

Step 4: Compute the fused estimates,

$$\hat{\xi}_{k|k} = \sum_{j=1}^{M} \hat{\xi}_{k|k}^{(i)} \mu_k^{(i)} \tag{11}$$

$$\hat{\Sigma}_{k|k} = \sum_{i=1}^{M} [\Sigma_{k|k}^{(i)} + (\hat{\xi}_{k|k} - \hat{\xi}_{k|k}^{(i)})(\hat{\xi}_{k|k} - \hat{\xi}_{k|k}^{(i)})^T] \mu_k^{(i)} \tag{12}$$

Algorithm 1 Kalman filter equations for mode (i)

Inputs: $(\bar{\xi}_{k-1|k-1}^{(i)}, \bar{\Sigma}_{k-1|k-1}^{(i)})$
Prediction step:
$\hat{\xi}_{k|k-1}^{(i)} = F_{k-1}^{(i)} \bar{\xi}_{k-1|k-1}^{(i)} + E_{k-1}^{(i)}$
$\hat{\Sigma}_{k|k-1}^{(i)} = F_{k-1}^{(i)} \bar{\Sigma}_{k-1|k-1}^{(i)} F_{k-1}^{(i)^T} + G_{k-1}^{(i)} Q_{k-1}^{(i)} G_{k-1}^{(i)^T}$
Update step:
$\tilde{y}_k^{(i)} = y_k - H_k^{(i)} \hat{\xi}_{k|k-1}^{(i)}$
$S_k^{(i)} = H_k^{(i)} \hat{\Sigma}_{k|k-1}^{(i)} H_k^{(i)^T} + R_k^{(i)}$
$K_k^{(i)} = \hat{\Sigma}_{k|k-1}^{(i)} H_k^{(i)^T} S_k^{(i)^{-1}}$
$\hat{\xi}_{k|k}^{(i)} = \hat{\xi}_{k|k-1}^{(i)} + K_k^{(i)} \tilde{y}_k^{(i)}$
$\hat{\Sigma}_{k|k}^{(i)} = \hat{\Sigma}_{k|k-1}^{(i)} - K_k^{(i)} S_k^{(i)} K_k^{(i)^T}$
Outputs: $(\hat{\xi}_{k|k}^{(i)}, \hat{\Sigma}_{k|k}^{(i)}, \tilde{y}_k^{(i)}, S_k^{(i)})$

3.3 Target State Prediction

Recall that one of the main goals of the environment model is to forecast the state of the target vehicle over the prediction horizon of the controller. At time k, we first estimate the most likely mode m_k as the mode (i) with the highest probability $\mu_k^{(i)}$. Given the mode, the state is assumed to evolve according to the dynamics (1a). Note that the longitudinal and lateral state predictions are performed separately and later combined for the control design. The predicted positions of target vehicles are used to formulate constraints on the ego vehicle state. This is described later in Section 5.1.

4. VEHICLE MODEL

Starting from a nonlinear model in Section 4.1, we derive a linear parameter–varying (LPV) model of the vehicle dynamics in Section 4.2.

4.1 Nonlinear Bicycle Model

The notation used in the vehicle model is depicted in Figure 3. The following set of nonlinear differential equations are used to describe the motion of the vehicle in the road–aligned coordinate frame,

$$\ddot{x} = \dot{y}\dot{\psi} + a_x \tag{13a}$$
$$\ddot{y} = -\dot{x}\dot{\psi} + \frac{1}{m}(2F_{y,f} + 2F_{y,r}) \tag{13b}$$
$$\ddot{\psi} = \frac{1}{I_z}(2aF_{y,f} - 2bF_{y,r}) \tag{13c}$$
$$\dot{e}_\psi = \dot{\psi} - \kappa\dot{s} \tag{13d}$$
$$\dot{e}_y = \dot{x}sin(e_\psi) + \dot{y}cos(e_\psi) \tag{13e}$$

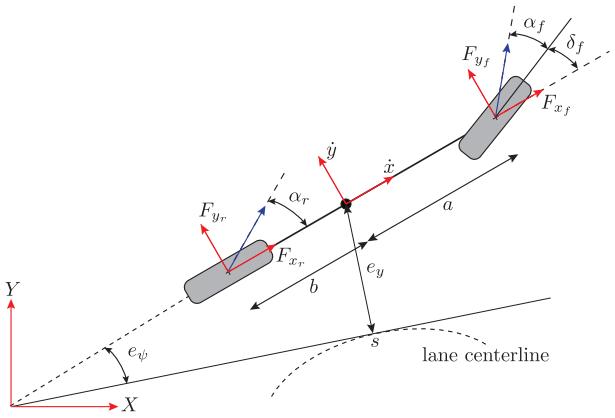

Fig. 3. Vehicle model notation

$$\dot{s} = \frac{1}{1-\kappa e_y}(\dot{x}cos(e_\psi) - \dot{y}sin(e_\psi), \tag{13f}$$

where m and I_z denote the vehicle mass and yaw inertia, respectively, a and b denote the distances from the vehicle's center of gravity to the front and rear axles, respectively. $\dot{x}$ and $\dot{y}$ denote the longitudinal and lateral speeds in the body frame, respectively, $\dot{\psi}$ denotes the yaw rate, and a_x denotes the commanded longitudinal acceleration. e_y and e_ψ denote the lateral position error and angular error with respect to the road centerline, respectively, κ denotes the curvature of the road, and s denotes the longitudinal position of the vehicle along the road. The lateral force in the body frame $F_{y,\star}$ ($\star \in \{f, r\}$) is given by,

$$F_{y,\star} = -C_\star \alpha_\star, \tag{14}$$

where $C_\star$ denotes the tire cornering stiffness, and $\alpha_\star$ denotes the lateral tire slip angle which is computed using small angle approximations as,

$$\alpha_f = -\delta_f + \frac{\dot{y} + a\dot{\psi}}{\dot{x}}, \quad \alpha_r = \frac{\dot{y} - b\dot{\psi}}{\dot{x}}, \tag{15}$$

where δ_f is the commanded front steering angle. The nonlinear bicycle model can be compactly written as,

$$\dot{\xi}(t) = f(\xi(t), u(t), p(t)), \tag{16}$$

where $\xi = [\dot{x}, \dot{y}, \dot{\psi}, e_\psi, e_y, s]^T$, $u = [\delta_f, a_x]^T$, and $p = \kappa$ are the state, input and parameter vectors, respectively.

4.2 Linear Parameter-Varying (LPV) Model

For the control design, we linearize the bicycle model described above around the current longitudinal speed to obtain an LPV model of the vehicle dynamics. The following assumptions are introduced,

Assumption 1: The angular error e_ψ is small, hence $sin(e_\psi) \approx e_\psi$, $cos(e_\psi) \approx 1$.

Assumption 2: The lateral velocity $\dot{y}$ and yaw rate $\dot{\psi}$ are small, hence $\dot{y}\dot{\psi} \approx 0$, $\dot{y}e_\psi \approx 0$.

Assumption 3: The road curvature κ is assumed to be known as a function of the longitudinal position s along the road.

Under these assumptions, the system dynamics (13) can be expressed as,

$$\dot{\xi}(t) = A_c(\rho(t))\xi(t) + B_c u(t), \tag{17}$$

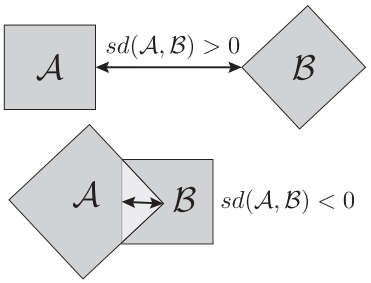

Fig. 4. Signed distance between convex shapes $\mathcal{A}$ and $\mathcal{B}$

where $\rho = [\dot{x}, \kappa]^T$ is the parameter vector about which the linearization is performed, and

$$A_c(\rho) = \begin{bmatrix} 0 & 0 & 0 & 0 & 0 & 0 \\ 0 & \frac{-2(C_f+C_r)}{m\dot{x}} & \frac{-2(aC_f-bC_r)}{m\dot{x}} & 0 & 0 & 0 \\ 0 & \frac{-2(aC_f-bC_r)}{I_z\dot{x}} & \frac{-2(a^2C_f+b^2C_r)}{I_z\dot{x}} & 0 & 0 & 0 \\ -\kappa & 0 & 1 & 0 & 0 & 0 \\ 0 & 1 & 0 & \dot{x} & 0 & 0 \\ 1 & 0 & 0 & 0 & 0 & 0 \end{bmatrix},$$

$$B_c = \begin{bmatrix} 0 & 1 \\ \frac{2C_f}{m} & 0 \\ \frac{2aC_f}{I_z} & 0 \\ 0 & 0 \\ 0 & 0 \\ 0 & 0 \end{bmatrix}.$$

In the following sections, we drop the dependence of A_c on ρ for visual clarity.

To account for uncertainties due to model mismatch and linearization errors, we introduce an additive stochastic disturbance in (17). The modified LPV model can be written in discrete–time as,

$$\xi_{k+1} = A_k\xi_k + B_k u_k + D_k w_k, \tag{18}$$

where $w_k \sim \mathcal{N}(0, \Sigma_w)$. Note that (18) is obtained by a forward Euler discretization of (17).

Remark 2: The data from [3] is used to estimate the disturbance covariance Σ_w

Remark 3: The LPV model was derived using a linear tire model approximation. The MPC approach presented in Section 6 can be directly applied to LTV models which use nonlinear tire models for the linearization [2].

5. SAFETY CONSTRAINTS

5.1 Collision avoidance

We employ an approach similar to that in [9] for formulating collision avoidance constraints. This is based on the notion of signed distance in collision detection literature, which is defined below.

Definition 1: Let $\mathcal{A}$ and $\mathcal{B}$ be convex shapes. The *signed distance* $sd(\mathcal{A}, \mathcal{B})$ is defined as the length of the smallest translation that puts the two shapes $\mathcal{A}$ and $\mathcal{B}$ (1) in contact, if they are currently separated *or* (2) out of contact, if they are currently in contact.

This is illustrated in Figure 4. Details about the signed distance and its computation are presented in [9]. Without loss of generality, we consider the case of

one moving target vehicle. Recall that the "Environment Model" block provides us with an estimate of the current and future positions of the target vehicle. At any time instant t, let the predicted position of the target vehicle at time $t+k$ be denoted as $\bar{\xi}^e_{t+k,t}$, and that of the ego vehicle be denoted as $\bar{\xi}_{t+k,t}$. Let the target vehicle be represented by a convex shape $\mathcal{T}_{t+k,t}$, and the ego vehicle by $\mathcal{E}_{t+k,t}$. Note that $\mathcal{T}_{t+k,t}$ and $\mathcal{E}_{t+k,t}$ are functions of $\bar{\xi}^e_{t+k,t}$ and $\bar{\xi}_{t+k,t}$, respectively. The collision avoidance constraint can be expressed as,

$$sd(\mathcal{T}_{t+k,t}, \mathcal{E}_{t+k,t}) \geq 0. \tag{19}$$

The above constraint is nonlinear and non–convex in general. We linearize (19) around the predicted ego vehicle state $\bar{\xi}_{t+k,t}$ to obtain

$$\begin{aligned} d_k + \nabla d_k \cdot \Delta\xi_k \geq 0, \\ (d_k = sd(\mathcal{T}_{t+k,t}, \mathcal{E}_{t+k,t})) \end{aligned} \tag{20}$$

where $\Delta\xi_k$ is the deviation of the ego vehicle state from $\bar{\xi}_{t+k,t}$. (20) can be expressed in the standard form of a linear inequality as

$$g_k^T \xi_{t+k,t} \leq h_k. \tag{21}$$

Note that the RHS of (21) is uncertain due to the uncertainty in the predicted target vehicle position. This is dealt with by suitably increasing the dimensions of $\mathcal{T}_{t+k,t}$ such that the target vehicle will be contained in $\mathcal{T}_{t+k,t}$ with a high probability. Moreover, the LHS is also uncertain due to the uncertainty in $\xi_{t+k,t}$ arising from the additive disturbance in (18). We account for this by formulating (21) as a chance–constraint to be satisfied with a specified probability p. That is,

$$Pr(g_k^T \xi_{t+k,t} \leq h_k) \geq p, \quad 0.5 \leq p \leq 1, \tag{22}$$

where p denotes the tunable risk parameter. Naturally, a large value of p would lead to conservative behavior, possibly making the chance–constrained optimal control problem (25) infeasible. On the other hand, a low value of p might lead to a higher risk of collision. The effect of varying p of the driving performance is studied in more detail in Section 7.

5.2 Lane boundaries

The requirement that the vehicle stays within the lane can be expressed as,

$$e^{lane}_{y,\min} \leq e_y \leq e^{lane}_{y,\max}, \tag{23}$$

where the bounds $e^{lane}_{y,\min}$ and $e^{lane}_{y,\max}$ account for the width of the vehicle.

5.3 Input constraints

Physical limitations on the actuators impose bounds on the control inputs and input rates,

$$u_{min} \leq u(t) \leq u_{max}, \quad \dot{u}_{min} \leq \dot{u}(t) \leq \dot{u}_{max}. \tag{24}$$

6. CONTROL DESIGN

6.1 Chance–constrained MPC

The vehicle model and safety constraints described above are used to formulate a chance–constrained receding horizon control problem. At each sampling time, a constrained finite–time optimal control problem is solved to determine a sequence of control inputs which minimizes a given cost function. Only the first input of the sequence is applied to the system. The process is repeated at the next sampling instant using new measurements. The optimization problem to be solved at each time step is given by,

$$\min_{\mathbf{u_t}} \sum_{k=0}^{H_p-1} \mathbb{E}(\|\xi_{t+k+1,t} - \xi_{ref,k+1}\|^2_Q + \|u_{t+k,t}\|^2_R) \tag{25a}$$

$$\text{s.t. } \xi_{t+k+1,t} = A_k \xi_{t+k,t} + B_k u_{t+k,t} + D_k w_k \tag{25b}$$

$$Pr(g^T_{k+1} \xi_{t+k+1,t} \leq h_{k+1}) \geq p \tag{25c}$$

$$(k = 0, \ldots, H_p - 1)$$

$$G_u \mathbf{u}_t \in \mathcal{U} \tag{25d}$$

$$\xi_{t,t} = \xi(t), \tag{25e}$$

where t denotes the current time instant, H_p denotes the prediction horizon and $\xi_{t+k,t}$ denotes the predicted ego vehicle state at time $t+k$ obtained by applying the control sequence $\mathbf{u_t} = \{u_{t,t}, u_{t+1,t}, \ldots, u_{t+H_p-1,t}\}$ to the vehicle model (25b) with initial condition $\xi_{t,t} = \xi(t)$. (25d) is a compact representation of the input constraints in (24). The reference state sequence $\{\xi_{ref,k}\}_{k=1}^{H_p}$ in (25a) encodes control objectives such as tracking the lane centerline and maintaining a desired speed.

The optimization problem (25) cannot be solved directly because of the presence of the stochastic disturbance w in (25b), and the chance–constraints (25c). The original constraints must be tightened to account for the state uncertainty at each time step in the horizon. This is presented below. The variables $\xi_{t+k,t}$ and $u_{t+k,t}$ are denoted as ξ_k and u_k, respectively, for visual clarity.

6.2 Closed–loop approach

We use the closed–loop paradigm introduced in [5] to decompose the state and input as,

$$\xi_k = z_k + e_k \tag{26a}$$

$$u_k = K_k \xi_k + c_k, \tag{26b}$$

where K_k is a stabilizing feedback gain for the pair (A_k, B_k), z_k denotes the deterministic component of ξ_k, and e_k denotes the stochastic component. c_k represents perturbations on a given feedback control law. Substituting for ξ_k and u_k in (25b) gives,

$$z_{k+1} = \Phi_k z_k + B_k c_k \tag{27a}$$

$$e_{k+1} = \Phi_k e_k + D_k w_k, \tag{27b}$$

where $\Phi_k = A_k + B_k K_k$. We introduce the following assumptions,

Assumption 4: The system has perfect state feedback, i.e., $\xi_0 = z_0$. This implies $e_0 = 0$ with probability 1.

Assumption 5: The pair (A_k, B_k) is controllable. Hence, there exists K_k such that Φ_k is Hurwitz.

Remark 4: K_k is chosen to be the infinite horizon LQR gain for (A_k, B_k).

6.3 Uncertainty Propagation

The separation of the deterministic and stochastic components of ξ_k in (26) allows us to determine the distributions of e_k $(k = 1, \ldots, H_p)$ knowing the distributions of e_0 and w_k. Let $e_k \sim \mathcal{N}(0, \Sigma_k)$. Then, $e_{k+1} \sim \mathcal{N}(0, \Sigma_{k+1})$, where

$$\Sigma_{k+1} = \Phi_k \Sigma_k \Phi_k^T + D_k \Sigma_w D_k^T. \tag{28}$$

The initial condition is $\Sigma_0 = 0$ by Assumption 4.

6.4 Constraint Tightening

Based on (26), the probabilistic constraint (25c) becomes

$$Pr(g_k^T z_k + g_k^T e_k \leq h_k) \geq p. \quad (k = 1, \ldots, H_p) \tag{29}$$

This is satisfied if [5],

$$g_k^T z_k \leq h_k - \gamma_k \tag{30a}$$

$$Pr(g_k^T e_k \leq \gamma_k) = p \tag{30b}$$

Since we know that $g_k^T e_k \sim \mathcal{N}(0, g_k^T \Sigma_k g_k)$, we can explicitly compute γ_k from the quantile function of a univariate normal distribution as

$$\gamma_k = \sqrt{2 g_k^T \Sigma_k g_k}\ erf^{-1}(2p - 1) \tag{31}$$

where $erf^{-1}(\cdot)$ is the inverse error function.

6.5 Modified Optimization Problem

By replacing (25c) with the tightened constraints (30a) and using the feedback law (27b), we obtain the following optimization problem to be solved at each time step,

$$\min_{\mathbf{c}} \sum_{k=0}^{H_p-1} \|z_{k+1} - \xi_{ref,k+1}\|_Q^2 + \|K_k z_k + c_k\|_R^2 \tag{32a}$$

$$\text{s.t. } z_k = A_k z_k + B_k c_k \tag{32b}$$

$$g_k^T z_k \leq h_k - \gamma_k \quad (k = 0, \ldots, H_p - 1) \tag{32c}$$

$$G_u(\mathbf{K}\mathbf{z} + \mathbf{c}) \in \mathcal{U} \tag{32d}$$

$$z_0 = \xi(t), \tag{32e}$$

where,

$$\mathbf{K} = blkdiag(K_0, \ldots, K_{H_p-1})$$
$$\mathbf{z} = [z_0, \ldots, z_{H_p-1}]^T$$
$$\mathbf{c} = [c_0, \ldots, c_{H_p-1}]^T.$$

(32) is a quadratic program (QP) which can be solved efficiently in real–time. Note that (32c) is implemented as a soft constraint to prevent the QP from becoming infeasible.

7. RESULTS

7.1 Simulation setup

Simulations are performed in MATLAB, and the constrained optimization problem (32) is solved using Gurobi [10]. The controller is connected in closed–loop with a higher fidelity four–wheel nonlinear model (which uses a Pacejka tire model) to simulate model mismatch.

7.2 Test scenario

The scenario consists of two target vehicles (denoted as T_1 and T_2) on a straight road. At the start of the simulation, T_1 is in the right lane moving at a speed of 6 m/s. It performs a lane change maneuver at approximately 3 seconds, and moves into the left lane. T_2 starts in the right lane at a speed of 8 m/s, and stays in the right lane for the entire duration of the simulation. The ego vehicle (denoted as E) starts off in the left lane, just behind T_1 and T_2, at a speed of 10 m/s. It's goal is to track the left lane, while maintaining a speed of 15 m/s. T_1 and T_2 are assumed to move with a constant velocity of 6 and 8 m/s, respectively, perturbed by the sum of a low–frequency sinusoidal term and a Gaussian disturbance. The lane change trajectory for T_1 is generated using a sigmoid function.

7.3 Results

To illustrate the effectiveness of the controller, we show snapshots of the simulation at various time instants in Figure 5. In each sub–figure, the red boxes depict the current positions of the ego vehicle E and target vehicles T_1 and T_2, while the gray boxes depict the predicted positions. The predicted positions of E are obtained from the MPC, and those of T_1 and T_2 are given by the IMM–KF. The red dashed lines for each target depict the ground truth positions. As seen in Figure 5(a), the IMM–KF predicts a lane change maneuver for T_1. This results in the E slowing down (Figure 5(b)). In Figure 5(c), E tries to plan a path around T_1, but is prevented from doing so by the presence of T_2. Finally, in Figure 5(e), we see that E is able to plan a path in between T_1 and T_2, and increase its speed.

In addition, we demonstrate the ability of the environment model to predict the lane change intention of T_1 by plotting the lateral mode probabilities in Figure 6. For visual clarity, the lateral modes are classified into two categories, "Right Lane" and "Left Lane". The probabilities for each category are shown in Figure 6 for part of the simulation. It is observed that as T_1 starts moving towards the left, the probability of the "Left Lane" mode increases while that of the "Right Lane" mode decreases.

7.4 Risk vs. conservativeness

An important element of the stochastic MPC problem is the risk parameter p, defined as the probability of violating the chance–constraints (22). The nominal MPC problem where the disturbances are assumed to be zero is given by $p = 0.5$. We would like to study the effect of varying p on the performance of the controller.

For the scenario described in Section 7.2, the distance traveled by the ego vehicle E in 25 seconds is used as

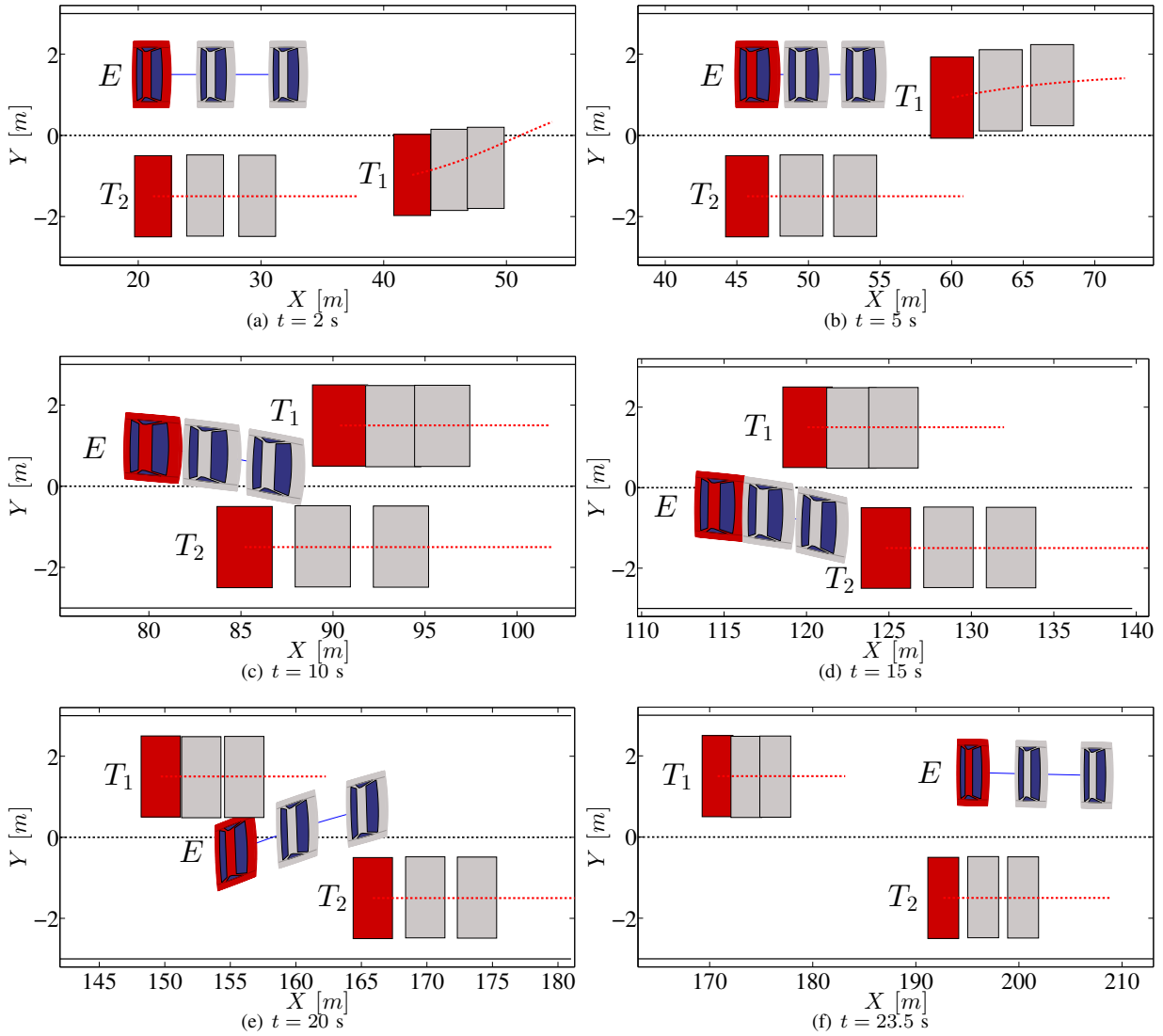

Fig. 5. Snapshots of simulation with current and predicted positions of ego vehicle E and target vehicles T_1 and T_2. The red boxes depict the current positions, while the gray boxes depict the future positions. For each target vehicle, the ground truth is shown by the dashed red line.

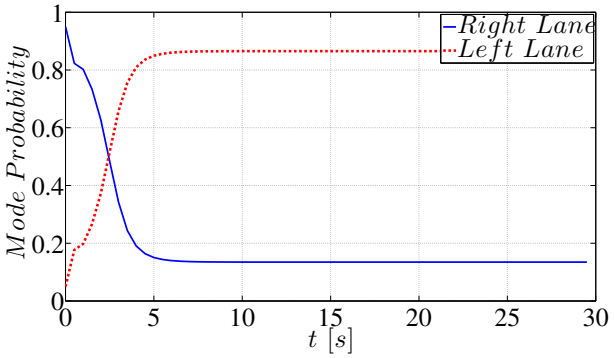

Fig. 6. Mode probabilities for target vehicle T_1 which changes lanes in front of the ego vehicle

the comparison metric. It is seen that E travels about 214 m with $p = 0.998$, and about 220 m with $p = 0.5$. Although the difference is small, it must be noted that the scenario presented is simple. For more complex scenarios encountered in day–to–day commutes, the difference in travel distances (and hence, travel times) can be much larger.

Another simple scenario gives insight on the effect of varying p on the conservatism of the controller. The scenario consists of a slow target vehicle T_1 moving in the left lane at a speed of 5 m/s, and a faster vehicle T_2 moving in the right lane at a constant speed of 9 m/s. The ego vehicle E starts in the left lane with a speed of 10 m/s.

The initial positions of E, T_1 and T_2 are chosen such that the nominal MPC with no constraint tightening ($p = 0.5$) is able to plan a path around T_1 while avoiding a collision with T_2, as shown in Figure 7(a). On the other hand, the chance–constrained MPC with $p = 0.998$ results in the ego vehicle slowing down significantly to wait for T_2 to pass before going around T_1. A snapshot of the simulation with the chance–constrained MPC is shown in Figure 7(b). The variation in the distance traveled by the ego vehicle with p is more significant in this case. For the nominal MPC with $p = 0.5$, the ego vehicle travels about 278 m in 20 seconds, while in

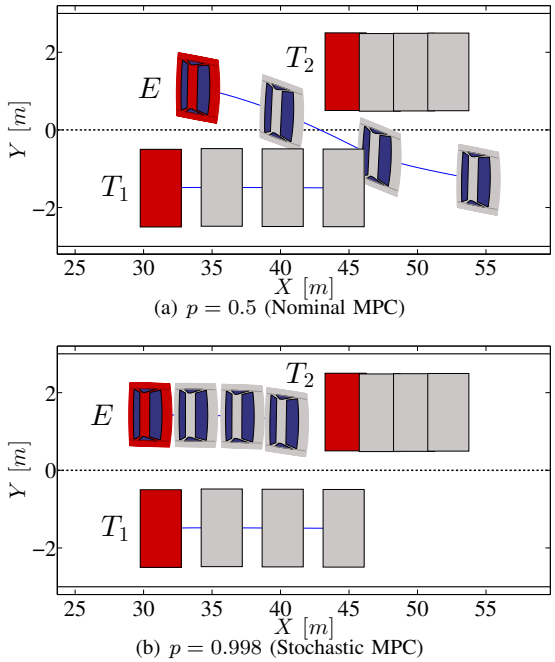

(a) $p = 0.5$ (Nominal MPC)

(b) $p = 0.998$ (Stochastic MPC)

Fig. 7. Simulation showing the effect of varying the risk parameter p on the conservatism of the controller. The notation is the same as in Figure 5

case of the chance–constrained MPC with $p = 0.998$, it covers only 193 m.

In the context of urban driving, scenarios like the one described above are expected to occur often. The use of conservative worst–case approaches may result in the ego vehicle stopping or slowing down unnecessarily, leading to longer commute times. The framework proposed in this work is expected to be less restrictive, while retaining the ability to systematically account for system uncertainties.

8. CONCLUSIONS

In this paper, we presented the integration of an environment model with a stochastic predictive control approach for autonomous vehicles. A multimodal approach is used to estimate and predict the state of surrounding vehicles. The predictions are embedded in a chance–constrained MPC which optimizes control inputs to achieve certain objectives while avoiding collisions with other vehicles. The ability of the ego vehicle to safely traverse a typical urban driving scenario is demonstrated through simulation. In addition, we studied the effect of the tunable risk parameter in the stochastic MPC on the performance of the autonomous vehicle. The proposed framework allows us to vary the conservatism of the controller as a function of risk. Future work aims at exploring this relationship in greater detail.

9. ACKNOWLEDGMENTS

This material is based upon work supported by the National Science Foundation under Grant No. 1239323. Any opinions, findings, and conclusions or recommendations expressed in this material are those of the authors and do not necessarily reflect the views of the National Science Foundation.

REFERENCES

[1] A. Gray, Y. Gao, J. K. Hedrick, and F. Borrelli, "Stochastic predictive control for semi-autonomous vehicles with an uncertain driver model," in *Intelligent Transportation Systems (ITS), IEEE Conference on*, 2013.

[2] A. Carvalho, Y. Gao, A. Gray, H. E. Tseng, and F. Borrelli, "Predictive control of an autonomous ground vehicle using an iterative linearization approach," in *Intelligent Transportation Systems (ITS), IEEE Conference on*, 2013.

[3] Y. Gao, A. Gray, H. E. Tseng, and F. Borrelli, "A tube-based robust nonlinear predictive control approach to semiautonomous ground vehicles," *Vehicle System Dynamics*, 2014.

[4] M. P. Vitus and C. J. Tomlin, "A probabilistic approach to planning and control in autonomous urban driving," in *Proceedings of the 52nd IEEE Conference on Decision and Control*, Florence, Italy, December 2013.

[5] B. Kouvaritakis, M. Cannon, S. V. Raković, and Q. Cheng, "Explicit use of probabilistic distributions in linear predictive control," *Automatica*, vol. 46, no. 10, pp. 1719–1724, 2010.

[6] S. Lefèvre, D. Vasquez, and C. Laugier, "A survey on motion prediction and risk assessment for intelligent vehicles," *Robomech Journal*, to appear.

[7] E. Mazor, A. Averbuch, Y. Bar-Shalom, and J. Dayan, "Interacting multiple model methods in target tracking: a survey," *Aerospace and Electronic Systems, IEEE Transactions on*, vol. 34, no. 1, pp. 103–123, 1998.

[8] R. R. Pitre, V. P. Jilkov, and X. R. Li, "A comparative study of multiple-model algorithms for maneuvering target tracking," in *Defense and Security*. International Society for Optics and Photonics, 2005, pp. 549–560.

[9] J. Schulman, J. Ho, A. Lee, I. Awwal, H. Bradlow, and P. Abbeel, "Finding locally optimal, collision-free trajectories with sequential convex optimization," in *Robotics: Science and Systems (RSS)*. Citeseer, 2013.

[10] *Gurobi Optimizer Reference Manual*, Gurobi Optimization, Inc., 2014. [Online]. Available: http://www.gurobi.com